Stereodynamical Control of Cold Collisions between Two Aligned D_2 Molecules

Pablo G. Jambrina*
Departamento de Química Física, Universidad de Salamanca, Salamanca 37008, Spain

James F. E. Croft†
The Dodd-Walls Centre for Photonic and Quantum Technologies, Dunedin 9054, New Zealand and Department of Physics, University of Otago, Dunedin 9054, New Zealand

Junxiang Zuo and Hua Guo‡
Department of Chemistry and Chemical Biology, University of New Mexico, Albuquerque, New Mexico 87131, USA

Naduvalath Balakrishnan§
Department of Chemistry and Biochemistry, University of Nevada, Las Vegas, Nevada 89154, USA

F. Javier Aoiz‖
Departamento de Química Física, Universidad Complutense. Madrid 28040, Spain

(Received 24 July 2022; revised 25 September 2022; accepted 21 December 2022; published 19 January 2023)

Resonant scattering of optically state-prepared and aligned molecules in the cold regime allows the most detailed interrogation and control of bimolecular collisions. This technique has recently been applied to collisions of two aligned *ortho*-D_2 molecules prepared in the $j = 2$ rotational level of the $v = 2$ vibrational manifold using the Stark-induced adiabatic Raman passage technique. Here, we develop the theoretical formalism for describing four-vector correlations in collisions of two aligned molecules and apply our approach to state-prepared $D_2(v = 2, j = 2) + D_2(v = 2, j = 2) \rightarrow D_2(v = 2, j = 2) + D_2(v = 2, j = 0)$ collisions, making possible the simulations of the experimental results from first principles. Key features of the experimental angular distributions are reproduced and attributed primarily to a partial wave resonance with orbital angular momentum $\ell = 4$.

DOI: 10.1103/PhysRevLett.130.033002

In molecular encounters collision outcomes are influenced by factors such as the collision energy (E_{coll}) and directional properties (orientation and alignment). While measurements of the energy (actually, the kinetic temperature T) dependence of the collision rates are rather routine, experiments that measure the outcome of a molecular collision on the initial alignments of the reactants (stereodynamics) are scarce (see, for example, Refs. [1–19]).

Optical state preparation using the Stark-induced adiabatic Raman passage (SARP) method combined with coexpansion of the colliding species has become a versatile tool to explore the stereodynamics of atom-molecule and molecule-molecule collisions [11–13,18–21]. When applied to light molecules such as HD and D_2, relative collision energies near ~1 K can be achieved, as demonstrated for HD + H_2/D_2 [11,12], HD + He [19], and D_2 + He [13,18] mixtures. In this regime, isolated resonances control the collision outcome, and their strength sometimes depends on the relative alignment between the two partners [22–30], so the SARP method provides a powerful technique to study and control stereodynamics of bimolecular collisions. However, most of these studies involve atom plus molecule collisions, and those that deal with collisions between two molecules could only control the direction of the internuclear axis of one of the colliding partners [11,12].

Very recently, Zhou *et al.* [31] reported results of the inelastic collisions between two aligned *ortho*-$D_2(v = 2, j = 2)$ molecules prepared by the SARP technique, showing how the angular distribution of the scattered products depends sensitively on the direction of D_2 internuclear axis with regard to the scattering frame defined by $\boldsymbol{k}$ and $\boldsymbol{k}'$, the reactant-approach and product-recoil directions. Further, while not directly observed, key features of the angular distribution were attributed to a resonance caused by the orbital angular momentum $\ell = 2$ near 1 K in the incoming channel whose properties are predicted to be strongly influenced by the initial alignment of the two molecules.

Previous theoretical treatments of the stereodynamics of collisions between two molecules considered only the polarization of one of the collision partners [22–24,29,32,33], which are not adequate to describe collisions when both partners are polarized. While the effect of entangled-assisted coherent control has been discussed [34–36], it does not directly relate to the SARP experiments. Here, we present the theoretical formalism for the angular distribution

of scattered products when both collision partners are polarized. This formalism provides the quantum mechanical framework to understand four-vector correlations in molecular collisions, and is completely general for molecule-molecule collisions. Combining this formalism with full-dimensional quantum scattering calculations on an accurate *ab initio* potential energy surface (PES) [37], we reproduce the experimental angular distributions reported by Zhou *et al.* [31]. Agreement with experiments is only obtained when collisions involving two polarized molecules (both in $v = 2$) as well as one polarized (in $v = 2$) and one unpolarized molecule (in $v = 0$, also present in the beam) are considered. Our results reveal that there is an $\ell = 4$ partial wave resonance whose contribution to the experimental angular distribution is dominant in the 1.5–3.5 K collision energy range.

Let us consider collisions involving two molecules A and B, each of them in a pure rotational state j_A and j_B and that we can control the spacial distribution of the internuclear axis of one of them (for example, A). In that case, the state-to-state differential cross section (DCS) can be calculated as [32]

$$d\sigma(\theta|\beta,\alpha) = \sum_{k=0}^{2j}\sum_{q=-k}^{k}(2k+1)[U_q^{(k)}(\theta)]^* a_q^{(k)}, \quad (1)$$

where $a_q^{(k)}$ are the extrinsic polarization parameters that describe the anisotropic preparation of the collision partner in the $\boldsymbol{k}$–$\boldsymbol{k}'$ scattering frame. If A is prepared in a pure $|j_A m = 0\rangle$ state, where m is the magnetic quantum number with respect to a laboratory-fixed quantization axis (the polarization vector of the Stokes and pump laser in the SARP experiment), the polarization parameters $a_q^{(k)}$ are given by

$$a_q^{(k)} = C_{kq}(\beta,\alpha)A_0^{(k)} = C_{kq}(\beta,\alpha)\langle j_A 0, k0|j_A 0\rangle, \quad (2)$$

where $A_0^{(k)}$ are the extrinsic polarization parameters in the laboratory frame, C_{kq} are the modified spherical harmonics, whose arguments β and α are the polar and azimuthal angles that define the direction of the polarization vector in the scattering frame, and $\langle .., ..|..\rangle$ is the Clebsch-Gordan coefficient. For an isotropic internuclear axis distribution, the only nonzero $a_q^{(k)}$ element is $a_0^{(0)}$.

In Eq. (1), $U_q^{(k)}(\theta)$ are the intrinsic polarization dependent DCSs (PDDCSs) of the $\{\boldsymbol{k} - \boldsymbol{j}_A - \boldsymbol{k}'\}$ three-vector correlations that describe how the collision outcome depends on the relative geometry of the collision partners. $U_q^{(k)}(\theta)$ can be expressed in terms of the scattering amplitudes in the helicity representation, $f_{j'_A m'_A j'_B m'_B j_A m_A j_B m_B}(\theta) \equiv F_{m'_A m'_B m_A m_B}(\theta)$, as

$$U_q^{(k)}(\theta) = \frac{1}{(2j_A+1)(2j_B+1)}\sum_{\substack{m'_A,m'_B\\ m_A,m_B}} F_{m'_A m'_B m_A m_B}(\theta) \times F^*_{m'_A m'_B (m_A+q) m_B}(\theta)\langle j_A m_A, kq|j_A m_A + q\rangle, \quad (3)$$

with

$$F_{m'_A m'_B m_A m_B}(\theta) = \frac{\sqrt{(1+\delta_{v_A v_B}\delta_{j_A j_B})(1+\delta_{v'_A v'_B}\delta_{j'_A j'_B})}}{2ik} \times \sum_J (2J+1) d^J_{m'_A+m'_B, m_A+m_B}(\theta) \times S^J_{m'_A m'_B m_A m_B}(E), \quad (4)$$

where $d^J_{m'_A+m'_B,m_A+m_B}(\theta)$ is an element of the Wigner reduced rotation matrix, and S is an element of the scattering matrix in the helicity representation, with m'_A, m'_B, m_A, and m_B being the projections of j'_A, j'_B, j_A, and j_B on the initial and final relative velocities, respectively (the primed indices indicate the products states). The $\sqrt{(1+\delta_{v_A v_B}\delta_{j_A j_B})(1+\delta_{v'_A v'_B}\delta_{j'_A j'_B})}$ factor only applies to inelastic scattering between indistinguishable particles [38].

For two polarized reagents under the same polarization vector, the DCS can be expressed as

$$d\sigma(\theta|\beta,\alpha) = \sum_{k_A=0}^{2j_A}\sum_{q_A}\sum_{k_B=0}^{2j_B}\sum_{q_B}(2k_A+1)(2k_B+1) \times \left[U^{(k_A,k_B)}_{q_A,q_B}(\theta)\right]^* a^{(k_A)}_{q_A} a^{(k_B)}_{q_B}, \quad (5)$$

where each of the $a_q^{(k)}$ can be evaluated according to Eq. (2) as a function of the β and α angles. The intrinsic $\{\boldsymbol{k} - \boldsymbol{j}_A - \boldsymbol{j}_B - \boldsymbol{k}'\}$ four-vector PDDCSs $U^{(k_A,k_B)}_{q_A,q_B}$ can be calculated as

$$U^{(k_A,k_B)}_{q_A,q_B}(\theta) = \frac{1}{(2j_A+1)(2j_B+1)} \times \sum_{\substack{m'_A,m'_B\\ m_A,m_B}} F_{m'_A m'_B m_A m_B}(\theta) F^*_{m'_A m'_B (m_A+q_A)(m_B+q_B)}(\theta) \times \langle j_A m_A, k_A q_A|j_A(m_A+q_A)\rangle \times \langle j_B m_B, k_B q_B|j_B(m_B+q_B)\rangle. \quad (6)$$

If either k_A or k_B is zero, we recover the three-vector PDDCS $U_q^{(k)}(\theta)$. If $k_A = k_B = 0$, we recover the $U_0^{(0)}(\theta)$, the isotropic DCS.

The DCS in the SARP experiments that we aim to reproduce involves integration over the azimuthal angle (α). This allows us to simplify Eq. (5) to

$$d\sigma(\theta|\beta) = 2\pi\sum_{k_A,k_B}(2k_A+1)(2k_B+1)U^{(k_A,k_B)}_{0,0}(\theta)a_0^{(k_A)}a_0^{(k_B)}. \quad (7)$$

The coupled-channel quantum calculations to evaluate the scattering matrices are carried out in full dimensionality using a modified version of the TwoBC code [39] and the recently reported full-dimensional PES for the H_2-H_2

system [37]. This PES was developed by fitting energy points from multireference configuration interaction calculations using a permutationally invariant neural network method [40] with the proper electrostatic and long-range dispersion terms. Details of the scattering calculations are given in our prior works [22,23,41]. For pure rotational quenching of $D_2(v=2, j=2)$, results are insensitive to the inclusion of additional rotational or vibrational levels beyond $v=2$ and $j=4$ in the basis set.

In their experiments, Zhou *et al.* [31] used a collimated D_2 beam with a rotational temperature of ~130 K (see Supplemental Material [42]). Using SARP, nearly all $|v=0, j=0\rangle \equiv |0\ 0\rangle$ molecules are transferred to a $|2\ 2\rangle$ state. As a result of the pumping process, the internuclear axis of D_2 molecules in the $|2\ 2\rangle$ state is aligned in a chosen direction with respect to the molecular beam axis. Here, we will consider three possible scenarios: isotropic (no alignment) internuclear axis distribution, internuclear axis aligned parallel to the molecular beam axis ($\beta = 0°$ or HSARP), and internuclear axis aligned perpendicular to the molecular beam axis ($\beta = 90°$ or VSARP). After state preparation, D_2 molecules in the $|2\ 2\rangle$ state experience collisions with themselves and with other D_2 molecules in the beam giving rise to a pure rotational deexcitation to the $|2\ 0\rangle$ state whose angular distribution is selectively detected.

Since all the D_2 molecules travel along the molecular beam spanning a relatively narrow velocity distribution, the *relative* velocity distribution corresponds to $E_{\rm coll} < 5$ K. D_2 in a $|2\ 0\rangle$ state can be produced from inelastic collisions between either two polarized $|2\ 2\rangle$ molecules or between one polarized $|2\ 2\rangle$ and one unpolarized $|0\ 1\rangle$ or $|0\ 2\rangle$ partner (higher rotational states had negligible populations in the molecular beam). The excitation function (cross section as a function of $E_{\rm coll}$), $\sigma(E_{\rm coll})$, for each of these processes is shown in Fig. 1. For collisions between $|2\ 2\rangle$ and $|0\ 1\rangle$ or $|0\ 2\rangle$, $\sigma(E_{\rm coll})$ is characterized by a broad resonance peak at $E_{\rm coll} \sim 2.8$ K and a smaller peak around 2 K, both associated with $\ell = 4$ (see Fig. S1 in Supplemental Material [42]). Around the resonance, $\sigma(E)$ is larger for a HSARP preparation and slightly smaller for a VSARP preparation compared to the isotropic case. Away from the resonance, $\sigma(E)$ is similar for the three preparations of the $|2\ 2\rangle$ state. In contrast, $\sigma(E)$ for collisions between two $|2\ 2\rangle$ molecules displays a complex resonance structure centered around 2 K, which is also enhanced by the HSARP preparation. There is also a sharp resonance at $E_{\rm coll} \sim 1$ K that disappears for both HSARP and VSARP polarizations. All these resonances are associated mainly to $\ell = 4$ (see Fig. S1 in Supplemental Material [42]) and different values of the total angular momentum J. Collisions between two $|2\ 2\rangle$ molecules that lead to two $|2\ 0\rangle$ products, and those in which the unpolarized partner changes its rovibrational state, have a significantly smaller cross sections, and hence are not considered here. Irrespective of the $\sigma(E)$ shape, although

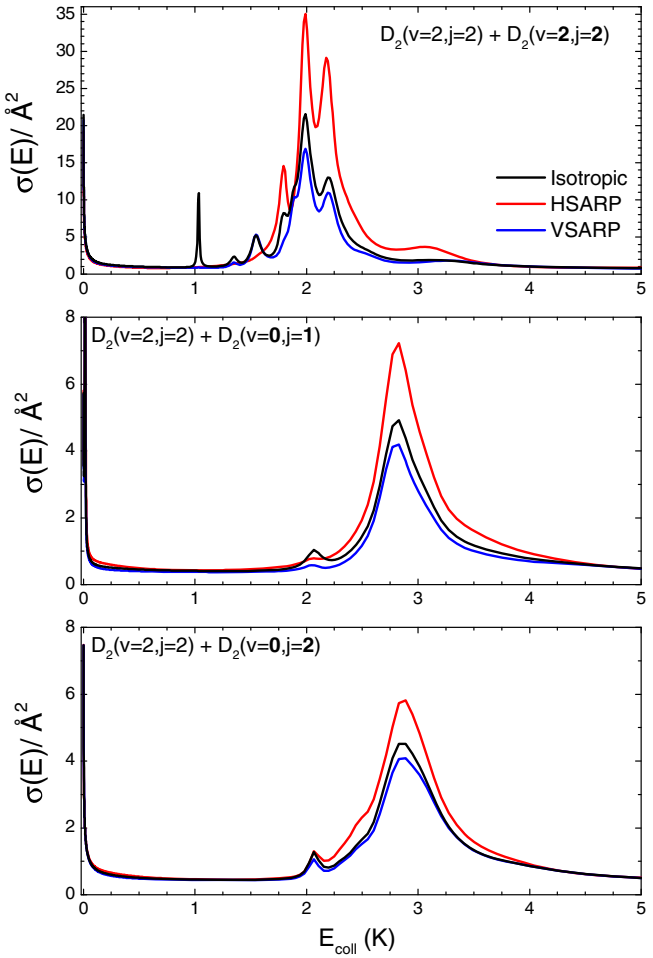

FIG. 1. Excitation functions for $D_2(v'=2, j'=0)$ production from $(v=2, j=2)+(v=2, j=2)$ collisions (top panel), $(v=2, j=2)+(v=0, j=1)$ (middle panel), and $(v=2, j=2)+(v=0, j=2)$ (bottom panel). Results for isotropic preparation is shown in black, while those for HSARP ($\beta = 0°$) and VSARP ($\beta = 90°$) are shown in red and blue, respectively.

the absolute values of the cross section for collisions between two $|2\ 2\rangle$ molecules are significantly larger at the energy of the resonance, all the three types of encounters have to be taken into account for the simulation of the experimental angular distributions.

Figure 2 depicts the energy dependent rate coefficients multiplied by the experimental $E_{\rm coll}$ distribution, such that its integral over $E_{\rm coll}$ is the rate coefficient. The higher flux for the HSARP preparation is consistent with its larger cross section compared to the VSARP preparation. The different contributions from the $v=2$ and $v=0$ quenchers are also highlighted. At $E_{\rm coll}$ within 1.5–2.5 K, the flux mostly originates from the resonance features due to $(v=2)+(v=2)$ collisions, whereas at higher energies the broad resonance due to $(v=2)+(v=0)$ collisions prevails. Overall, the energy distributions reflect the interplay between resonance features associated with $(v=2)+(v=2)$ and $(v=2)+(v=0)$ collision partners, all of

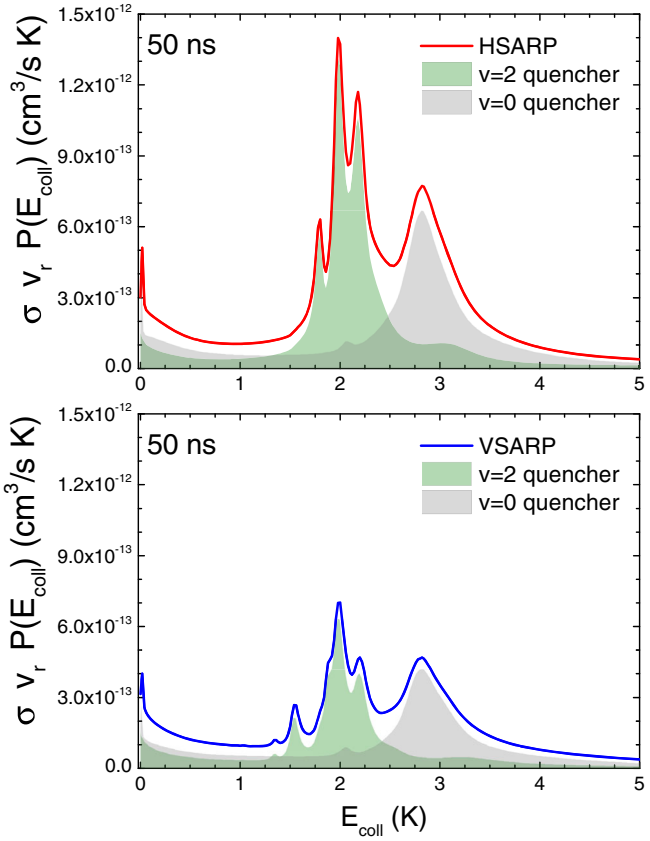

FIG. 2. Energy dependent integral rate coefficients multiplied by the experimental collision energy distribution for a 50 ns SARP REMPI delay time for the two experimental preparations: HSARP ($\beta = 0°$) (top panel) and VSARP ($\beta = 90°$) (bottom panel). The contribution of collisions between two $D_2(v = 2)$ molecules is highlighted in shaded dark green while that from collisions between one $D_2(v = 2)$ and one $D_2(v = 0)$ molecule is shown in shaded gray.

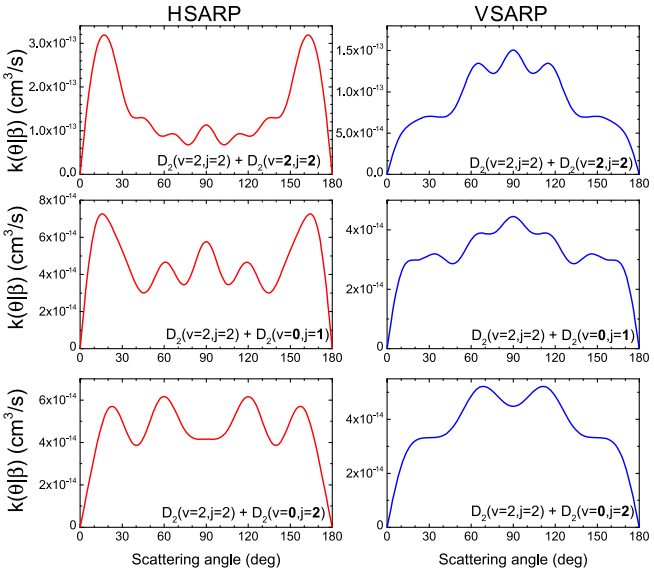

FIG. 3. Velocity-averaged differential rate coefficients for $D_2(v' = 2, j' = 0)$ production from $(v = 2, j = 2) + (v = 2, j = 2)$ collisions (top panel), $(v = 2, j = 2) + (v = 0, j = 1)$ (middle panel), and $(v = 2, j = 2) + (v = 0, j = 2)$ (bottom panel). Results for a HSARP (VSARP) preparation are shown in the left-hand (right-hand) panel. Differential rate coefficients were symmetrized as discussed in the text.

them associated to $\ell = 4$ (instead of $\ell = 2$ as discussed in Ref. [31]), and also show contributions from lower energies, associated to $\ell = 0$ and 1 (see Fig. S2 in Supplemental Material [42]). Scattering calculations were repeated assuming that D_2 internuclear distance is fixed at their vibrationally averaged values (see Fig. S4 in Supplemental Material [42]) leading to a small shift of the resonance peak toward lower E_{coll}. However, given the experimental E_{coll} distribution, this energy shift should not have a significant impact on the comparison with the experiment.

Figure 3 shows the computed angular distributions (differential rate coefficients) convolved over the experimental velocity distributions for the three collision pairs considered here and the HSARP and VSARP preparations. Since in the experiments it is not possible to distinguish between products scattered at θ or $\pi - \theta$ (where θ is the scattering angle, that between $\boldsymbol{k}$ and $\boldsymbol{k}'$), the angular distributions are symmetrized as in the experiments [31]. For HSARP preparations between two polarized $|2\ 2\rangle$ molecules we observe prominent peaks at 15° and 165°. These peaks are also present for $|2\ 2\rangle + |0\ 1\rangle$ collisions, although in that case, they are not that dominant, and peaks at 60°, 90°, and 120° also exist. For $|2\ 2\rangle + |0\ 2\rangle$ collisions the shape is similar but the magnitude is smaller for the forward and backward peaks. The sharp forward and backward peaks observed for $|2\ 2\rangle + |2\ 2\rangle$ are a consequence of the simultaneous polarization of both D_2 molecules, which is inherent to the experiment. If the simulation were carried out hypothetically considering polarization of only one of the two $D_2(v = 2, j = 2)$ partners, the two prominent forward or backward peaks in the experimental HSARP angular distribution cannot be accounted for (Fig. S3 [42]). For a VSARP preparation, we obtain a salient 90° peak for $|2\ 2\rangle + |2\ 2\rangle$ collisions that is somewhat suppressed for $|2\ 2\rangle + |0\ 1\rangle$ encounters. The angular distribution for $|2\ 2\rangle + |0\ 2\rangle$ collisions shows a small dip at 90° with small shoulders at each side at 70° and 110°.

Taking into account the populations of the different rovibrational states in the beam, it is possible to combine the angular distributions depicted in Fig. 3 and compare with the experimental angular distributions. Such a comparison is presented in Fig. 4. Note that experiments do not provide absolute values of DCS, so comparison is made on a relative scale. The agreement between experiment and calculations is good for both HSARP and VSARP. For HSARP our calculations predict that forward and backward experimental peaks are mainly caused by $|2\ 2\rangle + |2\ 2\rangle$ collisions while collisions between $|2\ 2\rangle + |0\ 1\rangle$

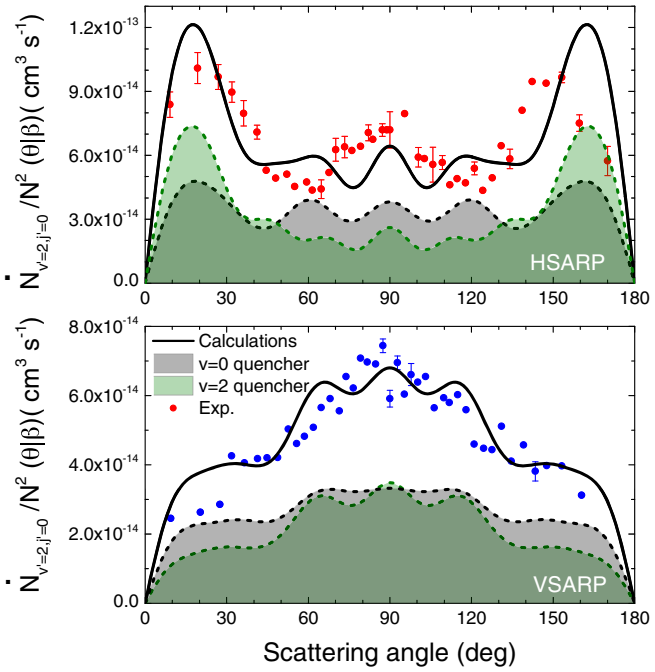

FIG. 4. Velocity-averaged differential rates for $D_2(v'=2, j'=0)$ production normalized by the square of the total density of D_2 (see Supplemental Material for further details [42]). Results of our calculations are shown in solid curves while experimental results of Zhou *et al.* [31] are shown in dots. Calculations using a HSARP (VSARP) preparation are shown in the top (bottom) panel. Differential rate coefficients were symmetrized as in the experimental work. The contribution of collisions between two $D_2(v=2)$ molecules is shown in shaded dark green, while that from collisions between one $D_2(v=2)$ and one $D_2(v=0)$ is shown in shaded gray and black dashed line.

and $|0\ 2\rangle$ have a more important contribution to sideways scattering and, in particular, to the smaller sideways peaks. Regarding VSARP, the experimental signatures primarily arise from the $|2\ 2\rangle + |2\ 2\rangle$ collisions modulated by small contributions from the other two collision pairs.

Altogether, our results provide a complete *ab initio* simulation of the experiments of Zhou *et al.* [31] on the stereodynamics of bimolecular collisions between two aligned D_2 molecules. This is enabled by developing the theory for stereodynamics of aligned-aligned bimolecular collisions and by considering different collision processes that occur in the molecular beam. Results presented here based on full-dimensional coupled-channel scattering calculations reveal that the angular distribution observed in the experiments of Zhou *et al.* [31] is due to resonance features that arise from different collision partners in the beam with distinct angular distributions. Key features of the experimental angular distributions are captured only when four-vector correlations in aligned-aligned molecular collisions are accounted for. The formalism presented here is general, and will provide the foundation for describing four-vector correlations in reactive or inelastic aligned molecular collisions in future experiments involving SARP or related techniques.

This work was supported in part by NSF Grant No. PHY-2110227 (N. B.) and ARO MURI Grant No. W911NF-19-1-0283 (N. B., H. G.). P. G. J. gratefully acknowledges Grant No. PID2020-113147GA-I00 funded by MCIN/AEI/10.13039/, and F. J. A. acknowledges funding by the Spanish Ministry of Science and Innovation (Grants No. PGC2018-096444-B-I00 and No. PID2021-122839NB-I00). J. F. E. C gratefully acknowledges support from the Dodd-Walls Centre for Photonic and Quantum Technologies.

*pjambrina@usal.es
†j.croft@otago.ac.nz
‡hguo@unm.edu
§naduvala@unlv.nevada.edu
‖aoiz@quim.ucm.es

[1] F. Wang, J. S. Lin, and K. Liu, Science **331**, 900 (2011).
[2] F. Wang, K. Liu, and T. P. Rakitzis, Nat. Chem. **4**, 636 (2012).
[3] F. Wang and K. Liu, J. Chem. Phys. **145**, 144305 (2016).
[4] F. Wang and K. Liu, J. Chem. Phys. **145**, 144306 (2016).
[5] M. Brouard, H. Chadwick, S. Gordon, B. Hornung, B. Nichols, F. J. Aoiz, and S. Stolte, J. Phys. Chem. A **119**, 12404 (2015).
[6] H. Chadwick, B. Nichols, S. D. S. Gordon, B. Hornung, E. Squires, M. Brouard, J. Kłos, M. H. Alexander, F. J. Aoiz, and S. Stolte, J. Phys. Chem. Lett. **5**, 3296 (2014).
[7] M. Brouard, H. Chadwick, C. J. Eyles, B. Hornung, B. Nichols, F. J. Aoiz, P. G. Jambrina, and S. Stolte, J. Chem. Phys. **138**, 104310 (2013).
[8] S. N. Vogels, T. Karman, J. Klos, M. Besemer, J. Onvlee, J. O. van der Avoird, G. C. Groenenboom, and S. Y. T. van de Meerakker, Nat. Chem. **10**, 435 (2018).
[9] J. Onvlee, S. D. S. Gordon, S. N. Vogels, T. Auth, T. Karman, B. Nichols, A. van der Avoird, G. C. Groenenboom, M. Brouard, and S. Y. T. van de Meerakker, Nat. Chem. **9**, 226 (2017).
[10] T. R. Sharples, J. G. Leng, T. F. M. Luxford, K. G. McKendrick, P. G. Jambrina, F. J. Aoiz, D. W. Chandler, and M. L. Costen, Nat. Chem. **10**, 1148 (2018).
[11] W. E. Perreault, N. Mukherjee, and R. N. Zare, Science **358**, 356 (2017).
[12] W. E. Perreault, N. Mukherjee, and R. N. Zare, Nat. Chem. **10**, 561 (2018).
[13] H. Zhou, W. E. Perreault, N. Mukherjee, and R. N. Zare, J. Chem. Phys. **154**, 104309 (2021).
[14] C. G. Heid, V. Walpole, M. Brouard, P. G. Jambrina, and F. J. Aoiz, Nat. Chem. **11**, 662 (2019).
[15] C. G. Heid, I. P. Bentham, V. Walpole, P. G. Jambrina, F. J. Aoiz, and M. Brouard, J. Phys. Chem. Lett. **12**, 310 (2021).
[16] C. G. Heid, I. P. Bentham, V. Walpole, R. Gheorge, P. G. Jambrina, F. J. Aoiz, and M. Brouard, Phys. Chem. Chem. Phys. **22**, 22289 (2020).

[17] V. Walpole, C. G. Heid, P. G. Jambrina, F. J. Aoiz, and M. Brouard, J. Phys. Chem. A **123**, 8787 (2019).
[18] H. Zhou, W. E. Perreault, N. Mukherjee, and R. N. Zare, Science **374**, 960 (2021).
[19] W. E. Perreault, N. Mukherjee, and R. N. Zare, J. Chem. Phys. **150**, 174301 (2019).
[20] C. Amarasinghe and A. G. Suits, J. Phys. Chem. Lett. **8**, 5153 (2017).
[21] C. Amarasinghe, C. A. Perera, and A. G. Suits, J. Chem. Phys. **152**, 184201 (2020).
[22] J. F. E. Croft, N. Balakrishnan, M. Huang, and H. Guo, Phys. Rev. Lett. **121**, 113401 (2018).
[23] J. F. E. Croft and N. Balakrishnan, J. Chem. Phys. **150**, 164302 (2019).
[24] P. G. Jambrina, J. F. E. Croft, H. Guo, M. Brouard, N. Balakrishnan, and F. J. Aoiz, Phys. Rev. Lett. **123**, 043401 (2019).
[25] M. Morita and N. Balakrishnan, J. Chem. Phys. **153**, 091101 (2020).
[26] M. Morita and N. Balakrishnan, J. Chem. Phys. **153**, 184307 (2020).
[27] M. Morita, Q. Yao, C. Xie, H. Guo, and N. Balakrishnan, Phys. Rev. Res. **2**, 032018(R) (2020).
[28] P. G. Jambrina, L. González-Sánchez, M. Lara, M. Menéndez, and F. J. Aoiz, Phys. Chem. Chem. Phys. **22**, 24943 (2020).
[29] P. G. Jambrina, J. F. E. Croft, N. Balakrishnan, and F. J. Aoiz, Phys. Chem. Chem. Phys. **23**, 19364 (2021).
[30] P. G. Jambrina, M. Morita, J. F. E. Croft, F. J. Aoiz, and N. Balakrishnan, J. Phys. Chem. Lett. **13**, 4064 (2022).
[31] H. Zhou, W. E. Perreault, N. Mukherjee, and R. N. Zare, Nat. Chem. **14**, 658 (2022).
[32] J. Aldegunde, M. P. de Miranda, J. M. Haigh, B. K. Kendrick, V. Saez-Rabanos, and F. J. Aoiz, J. Phys. Chem. A **109**, 6200 (2005).
[33] D. Yang, D. Xie, and H. Guo, J. Phys. Chem. Lett. **13**, 1777 (2022).
[34] J. Gong, M. Shapiro, and P. Brumer, J. Chem. Phys. **118**, 2626 (2003).
[35] A. Devolder, P. Brumer, and T. V. Tscherbul, Phys. Rev. Lett. **126**, 153403 (2021).
[36] A. Devolder, T. V. Tscherbul, and P. Brumer, Phys. Rev. A **105**, 052808 (2022).
[37] J. Zuo, J. F. E. Croft, Q. Yao, N. Balakrishnan, and H. Guo, J. Chem. Theory Comput. **17**, 6747 (2021).
[38] K. Takayanagi, Adv. At. Mol. Phys. **1**, 149 (1965).
[39] R. Krems, TwoBC—quantum scattering program, University of British Columbia, Vancouver, Canada, 2006.
[40] B. Jiang, J. Li, and H. Guo, Int. Rev. Phys. Chem. **35**, 479 (2016).
[41] G. Quéméner and N. Balakrishnan, J. Chem. Phys. **130**, 114303 (2009).
[42] See Supplemental Material at http://link.aps.org/supplemental/10.1103/PhysRevLett.130.033002 for further details about the calculation of initial molecular state and velocity-averaged differential rate coefficients, contribution of partial waves to the excitation functions, differences between three- and four-vector correlations, and comparison between rigid rotor and full-dimensional calculations, which includes Refs. [43,44].
[43] W. M. Huo and S. Green, J. Chem. Phys. **104**, 7572 (1996).
[44] D. L. Johnson, R. S. Grace, and J. G. Skofronick, J. Chem. Phys. **71**, 4554 (1979).